Structure and dynamics of the DNA-binding protein HU of *B. stearothermophilus* investigated by Raman and ultraviolet-resonance Raman spectroscopy[3]

DOINITA SERBAN,[1] SANDRA F. ARCINEIGAS,[1] CONSTANTINOS E. VORGIAS,[2] AND GEORGE J. THOMAS, JR.[1]

[1]Division of Cell Biology and Biophysics, School of Biological Sciences, University of Missouri-Kansas City, Kansas City, Missouri 64110-2499, USA
[2]National and Kapodistrian University of Athens, Faculty of Biology, Department of Biochemistry and Molecular Biology, Panepistimiopolis-Zographou, 157 84 Athens, Greece

(RECEIVED September 27, 2002; FINAL REVISION December 13, 2002; ACCEPTED January 7, 2003)

Abstract

The histone-like protein HU of *Bacillus stearothermophilus* (HUBst) is a 90-residue homodimer that binds nonspecifically to *B* DNA. Although the structure of the HUBst:DNA complex is not known, the proposed DNA-binding surface consists of extended arms that project from an α-helical platform. Here, we report Raman and ultraviolet-resonance Raman (UVRR) spectra diagnostic of subunit secondary structures and indicative of key side-chains lining the proposed DNA-binding surface. Raman conformation markers show that the DNA-binding arms of the dimer contain β-stranded structure in excess (eight ± two residues per subunit) of that reported previously. Important among side-chain markers are Met (701 cm^{-1}), Ala (908 cm^{-1}), Arg (1082 cm^{-1}), and Pro (1457 cm^{-1}). The Ala marker undergoes a substantial shift (908 → 893 cm^{-1}) on deuteration of alanyl peptide sites, indicating a coupled side-chain/main-chain mode of diagnostic value in the identification of exchange-protected alanines. A large subset of alanines (67%) in the α-helical core exhibits robust resistance to exchange. A quantitative study of NH → ND exchange exploiting newly identified amide II′ markers of helical (1440 cm^{-1}) and nonhelical (1472 cm^{-1}) conformations of HUBst indicates unexpected flexibility at the dimer interface, which is manifested in rapid exchange of 80% of peptide sites. The results establish a basis for subsequent Raman and UVRR investigations of HUBst:DNA complexes and provide a framework for applications to other DNA-binding architectural proteins.

Keywords: Architectural protein; structure; conformation; DNA binding; DNA recognition; Raman spectroscopy; amide II′; hydrogen exchange

[3]This article is part LXXXI in the series Raman Spectral Studies of Nucleic Acids.

Reprint requests to: George J. Thomas, Jr., Division of Cell Biology and Biophysics, School of Biological Sciences, University of Missouri-Kansas City, Kansas City, MO 64110-2499, USA; e-mail: thomasgj@umkc.edu; fax: (816) 235-1503.

Abbreviations: CD, circular dichroism; CM, carboxymethyl; ds, double-stranded; EDTA, ethylenediamine tetraacetic acid; GuDCl, guanidinium deuteriochloride; GuHCl, guanidinium hydrochloride; H/D, hydrogen/deuterium; HU, histone-like prokaryotic DNA-binding protein; HUBst, protein HU from *Bacillus stearothermophilus*; IHF, integration host factor; UVRR, ultraviolet-resonance Raman; LB, Luria-Bertani; IPTG, isopropyl-β-D-thiogalactoside; PLA, poly-L-arginine; PMSF, phenylmethylsulfonyl fluoride; SDS-PAGE, sodium dodecylsulfate–polyacrylamide gel electrophoresis; Tris, tris(hydroxymethylamino)methane.

Article and publication are at http://www.proteinscience.org/cgi/doi/10.1110/ps.0234103.

HU is the prototype of histone-like proteins that are abundant in all prokaryotes (~60,000 per cell) and bind DNA nonspecifically to bend the double helix (Drlica and Rouviere-Yaniv 1987; Rice 1997). The limited phylogenetic evolution of HU proteins is manifested in high sequence homology (up to 80%) among prokaryotes of the same genus (Drlica and Rouviere-Yaniv 1987; Wilson et al. 1990; Rice 1997; Esser et al. 1999). The locus of DNA binding is very highly conserved, indicating a common mechanism for DNA bending (White et al. 1989; Schneider et al. 1991). HU fulfills a pleiotropic role in bacterial gene regulation in vivo, functioning in the initiation of replication, posttranscriptional control, DNA repair, and condensation of DNA

into chromosome-like structures (Drlica and Rouviere-Yaniv 1987; Rice 1997; Bewley et al. 1998). Additionally, HU is required for the formation of recombinogenic complexes in multiple site-specific recombination reactions. In vitro, HU is observed to stabilize double-stranded (ds) DNA against thermal denaturation, a characteristic that may have a functional counterpart in vivo, particularly for thermophilic organisms (Esser et al. 1999).

HU proteins typically contain ~90 residues (molecular weight, ~10 kD). Both homodimeric and heterodimeric forms have been described (Drlica and Rouviere-Yaniv 1987). The structure of homodimeric HU from *Bacillus stearothermophilus* (HUBst) has been determined in both solution and crystal states (Boelens et al. 1996; White et al. 1999). The subunit N-terminal domain consists of two α-helices, which are interleaved with corresponding α-helices of a partner subunit to form a four-helix platform. The C-terminal domain of each subunit forms a largely antiparallel β-stranded fold, which projects from the helix platform. The two C-terminal folds of the dimer do not interact with one another but diverge to form arms (β-arms) suitable for grasping the DNA double helix (Fig. 1; Boelens et al. 1996; White et al. 1999).

Other DNA architectural proteins show large variations in sequence, binding specificity, and mechanism of DNA distortion (Luisi 1995; Werner et al. 1996; Williams and Maher III 2000). Three-dimensional structures solved to date indicate subunit side-chain intercalations into either the major or minor groove of the bound double helix as a mechanism that can bend or kink the DNA without significant perturbation of the protein scaffold (Werner et al. 1996). HU proteins engage the double helix at a convex surface, exposing multiple cationic side-chains (White et al. 1989; Rice et al. 1996; Williams and Maher III 2000). This surface, which provides electrostatic and steric complementarity for *B* DNA, has been confirmed as the nucleic acid binding site by mutational, biochemical, and biophysical assays (Saitoh et al. 1999). Arginines of the HUBst β-arms (Arg 53, Arg 55, Arg 58, Arg 61) are also highly conserved among HU proteins of different prokaryotes (Drlica and Rouviere-Yaniv 1987).

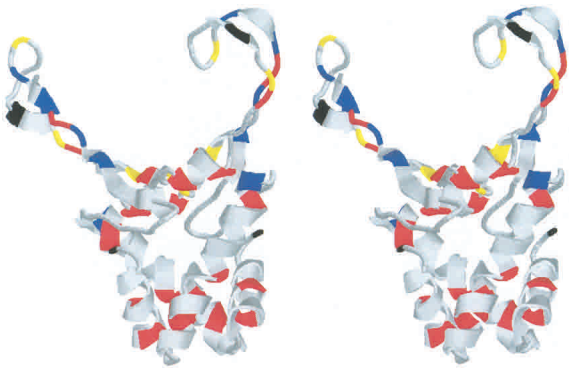

Figure 1. Stereo image of the NMR-determined three-dimensional structure of HUBst (Protein Data Bank entry 1HUE; Boelens et al. 1996). Locations of conserved residues (see text) are indicated in red (Ala), blue (Arg), yellow (Pro), and black (Met).

^{15}N-NMR chemical shifts of the HUBst:DNA complex indicate that several other side-chains on the inner surface of the β-arms (Met, Ile, Val, Asn, Gln) are also involved in DNA interactions (Boelens et al. 1996). Although no high-resolution structure is available for any HU:DNA complex, Pro, Met, and Ile side-chains are found consistently at the tips of the β-arms in the DNA-free structures. It has been proposed that these residues may function to "pry open" the minor groove and bend the DNA toward the major groove (Rice 1997; White et al. 1999). This proposal is supported by sequence and structure similarities between HUBst and the histone-like integration host factor (IHF). IHF is presently the only histone-like protein for which an X-ray crystal structure has been determined in a complex with DNA (Rice et al. 1996). IHF binds DNA both specifically and nonspecifically (Rice 1997; Holbrook et al. 2001), whereas most other histone-like proteins, including HUBst, bind nonspecifically (Drlica and Rouviere-Yaniv 1987). Differences in DNA-binding specificity among various histone-like proteins may be caused by differences in side-chains and their orientations along the putative DNA interface. Additional structural studies are required to identify such differences.

In this study, we report and interpret Raman and ultraviolet-resonance Raman (UVRR) spectra of HUBst. The data provide definitive vibrational assignments for the HUBst solution structure and represent the first comprehensive Raman analysis of a protein that is notably deficient in aromatic amino acid residues. The absence from HUBst Raman and UVRR spectra of the otherwise intense spectral markers expected from Tyr and Trp side-chains facilitates the identification of novel Raman markers of main-chain secondary structure and of key nonaromatic residues, including Ala, Arg, and Pro, which are of significance in DNA recognition. Finally, the present study establishes a foundation for future exploitation of Raman and UVRR spectroscopy to probe the structure and dynamics of HUBst:DNA complexes (D. Serban and G.J. Thomas, Jr., in prep.) and to further characterize DNA structural perturbations induced by specific and nonspecific DNA-binding proteins (Benevides et al. 2000a,b).

Results

Raman markers of HUBst secondary structure

Raman spectroscopy provides a convenient probe of the solution secondary structure of HUBst. The 532-nm excited Raman spectrum (Fig. 2, trace A) is distinguished by a strong and broad amide I band centered at 1658 cm^{-1} and

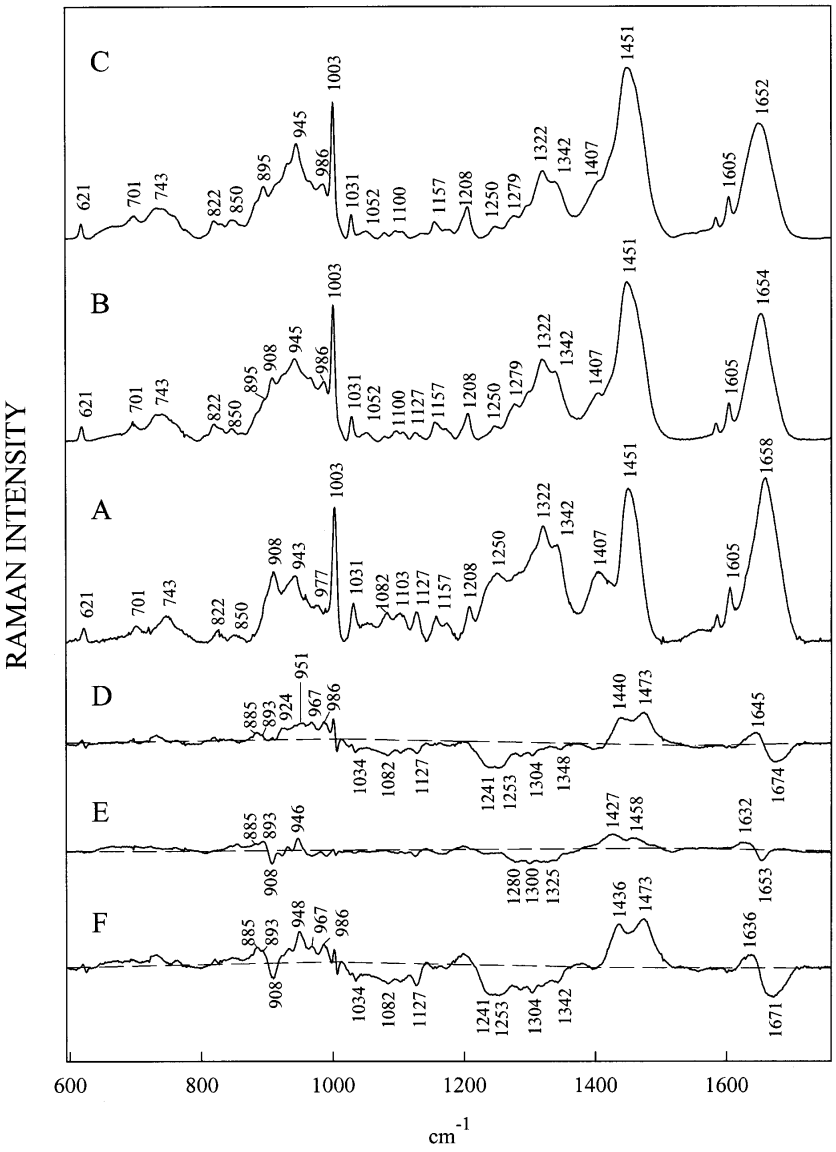

Figure 2. Raman spectra (600–1800 cm^{-1}, 532-nm excitation) of HUBst in H_2O and D_2O solutions at 20 mg/mL and 20 °C. (*A*) Native HUBst in 100 mM NaCl (pH 7.5). (*B*) Natively exchanged HUBst in 100 mM NaCl (pD 7.9). (*C*) Completely exchanged and natively refolded HUBst in 10 mM Tris, 50 mM NaCl (pD 7.9). (*D*) Difference spectrum (*B* – *A*) corresponding to exchange of unprotected sites of native HUBst. (*E*) Difference spectrum (*C* – *B*) corresponding to exchange of protected sites of native HUBst. (*F*) Difference spectrum (*C* – *A*) corresponding to complete exchange. *A*, *B*, and *C* were normalized to the integrated intensity of the phenylalanyl band near 1003 cm^{-1}, which is independent of deuteration (Overman and Thomas, Jr., 1998), and the normalized spectra were subtracted in *D*, *E*, and *F* to compensate the intensity of the 1003-cm^{-1} band.

a complex amide III profile, which includes a major peak at 1250 cm^{-1} and weaker shoulders at ~1241, 1279, and 1308 cm^{-1}. These are the Raman amide I and amide III features expected for a protein fold consisting of α-helix, β-strand, and irregular conformations (Miura and Thomas, Jr., 1995; Tuma and Thomas, Jr., 2001). A quantitative estimate of the HUBst secondary structure based on the Raman amide I reference intensity profile method (Berjot et al. 1987) indicates 36 ± 2% α-helix, 25 ± 3% β-strand, and 38 ± 3% irregular conformations (loops, turns, coils, and other aperiodic structures) for the dimer at 20°C. This method makes use of the fact that secondary structure contributions to the amide I band profile from α-helical, β-stranded, and irregular conformations, respectively, occur primarily near 1650 to 1655 cm^{-1}, 1665 to 1680 cm^{-1}, and 1655 to 1665 cm^{-1} (Miura and Thomas, Jr., 1995). The amide III envelope, which likewise comprises contributions from α-helix (1279 and 1308 cm^{-1}), β-strand (1241 cm^{-1}), and irregular conformations (1250 cm^{-1}), is consistent with the amide I analysis. The Raman results are also in accord with the

α-helix content of HUBst reported in previous NMR and X-ray studies (Boelens et al. 1996; White et al. 1999; Raves et al. 2001) and with the CD profile of HUBst in dilute solution (data not shown).

Raman monitoring of peptide NH → ND exchange

Raman spectral monitoring of peptide NH → ND exchange in proteins provides a basis for identifying domains that participate in inter-subunit contacts or undergo conformational changes along folding and assembly pathways (Tuma and Thomas, Jr., 1997; Tuma et al. 1999). Here, we use the method to distinguish HUBst domains that are either exchanged or protected in the native state. Figure 2 compares Raman spectra of the natively folded HUBst dimer in three isotopomeric forms: Trace A is the Raman signature of fully protiated (nonexchanged) HUBst; trace B is that of partially deuterated (natively exchanged) HUBst; and trace C is the signature of HUBst that is fully deuterated (refolded after complete exchange in 6 M GuDCl). Trace D (B − A) shows the computed Raman difference spectrum representing native exchange. The additional Raman differences resulting from exchange of domains that are protected in the native state are revealed in trace E (C − B). The cumulative effects of both native and unfolded exchanges are shown in trace F (C − A). All of the assigned Raman amide I/I′ and amide III/III′ markers (Table 1) are perturbed as expected by the peptide NH → ND exchanges of Figure 2. The salient findings and their interpretations are as follows.

The native-state deuteration shift of the composite amide I band (1658 → 1654 cm^{-1}) is resolved in the difference spectrum of Figure 2D as a peak/trough feature at 1645/1674 cm^{-1}. The trough component demonstrates that native-state exchange occurs predominantly at sites that are located in regions of β-strand or irregular secondary structure, that is, in non–α-helical domains of the native HUBst fold. On the other hand, the peptide sites that are protected in the native state but unprotected in the unfolded state occur primarily in α-helical domains, by virtue of the reduced amide I band intensity (difference trough) revealed at 1653 cm^{-1} in the difference spectrum of Figure 2E. The relative areas of the amide I difference troughs in Figure 2, D and E (~4:1), show further that in native HUBst the non–α-helical structure significantly exceeds the α-helical structure.

Secondary structures of natively exchanged and protected sites of HUBst can also be deduced from amide III/III′ difference features. Native exchange (Fig. 2D) is manifested in intense trough/peak features near 1240/986 cm^{-1} (β-strand) and 1255/924 cm^{-1} (irregular) and a weaker feature near 1305/951 cm^{-1} (α-helix). Conversely, subsequent exchange of unfolded HUBst (Fig. 2E) is dominated by the trough/peak pattern at 1300/946 cm^{-1} (α-helix). The amide III/III′ data are thus in agreement with the amide I/I′ results in demonstrating that exchange of the native HUBst fold occurs largely in non–α-helical regions, whereas the exchange-protected sites are located predominantly in α-helical regions (Miura and Thomas, Jr., 1995).

The relative intensities of amide III′ difference peaks in the 900- to 1000-cm^{-1} interval may also be used to estimate the populations of α-helical and non–α-helical sites undergoing peptide exchange (Tuma et al. 1996, 2001; Tuma and Thomas, Jr., 1997). We find that the integrated intensity of the amide III′ difference envelope in Figure 2D exceeds that of Figure 2E by roughly 4:1, implying in agreement with the amide I results that ~80% and ~20%, respectively, of HUBst residues are exchanged and protected in the native structure.

Many other difference features are also observed in the computed difference spectra of Figure 2. The most prominent of these is the Raman amide II′ band, which (unlike the vanishingly weak amide II band) exhibits significant intensity in Raman spectra of many deuterated proteins (Bandekar 1992; Tuma et al. 1996; Tuma and Thomas, Jr., 1997; Lee and Krimm 1998). In natively exchanged HUBst, the intense difference peaks near 1440 and 1473 cm^{-1} (Fig. 2D) are assigned collectively to amide II′ modes of all secondary structure types. The residues protected in the native structure but exchanged in the unfolded structure generate amide II′ peaks at 1427 and 1458 cm^{-1}. Although reliable secondary structure assignments have not previously been proposed for these amide II′ markers, we propose on the basis of the amide I/I′ and amide III/III′ results that the α-helical (exchange-protected) sites of HUBst generate amide II′ intensity in the 1427- to 1440-cm^{-1} interval, whereas non–α-helical (unprotected) sites generate amide II′ intensity in the 1458- to 1473-cm^{-1} interval.

Raman markers of alanine and effects of peptide exchange

Of additional interest in Figure 2 are difference bands resulting from the exchange of peptide sites of specific amino acid side-chains. Two types of exchange-sensitive bands of the side-chains can be distinguished: (1) bands representing localized vibrations of exchangeable sites (e.g., arginyl guanidinium modes that shift with $N^{\varepsilon}H$ or $N^{\eta}H$ deuteration, discussed below), and (2) bands representing coupled side-chain/main-chain vibrations. A well-studied example of the latter is the alanyl marker near 908 ± 2 cm^{-1}, which involves both C^{α}-C^{β} stretching and peptide N-H bending and therefore exhibits a small, but significant, shift to lower wavenumber (893 ± 2 cm^{-1}) with alanyl peptide deuteration (Sutton and Koenig 1970). The 908 → 893 cm^{-1} shift represents a specific Raman signature of alanyl NH → ND exchange. Thus, the trough/peak at 908/983 cm^{-1} in Figure 2F provides a benchmark for comparison of protected (Fig. 2E) and unprotected (Fig. 2D) alanyl NH sites. The data of Figure 2 show that the majority of alanyl NH sites are

Table 1. *Raman and UVRR frequencies, intensities, and assignments for protein HU from* Bacillus stearothermophilus *in H_2O and D_2O solutions*[a]

Raman cm^{-1}		Intensity		UVRR cm^{-1}		Intensity		
H_2O	D_2O	H_2O	D_2O	H_2O	D_2O	H_2O	D_2O	Assignment[b]
621	(621)	1	(1)	—	—	—	—	Phe (*F6b*)
701	(701)	1	(1)	—	—	—	—	ν(CS) trans χ^3
743	(743)	2	(2)	—	—	—	—	$\delta(CH_2)$, ν(CS) trans χ^3
822	(822)	1	(1)	—	—	—	—	ν(CC)
850	(850)	1	(1)	—	—	—	—	ν(CC)
908	(895)	4	3	—	—	—	—	$\nu(C^{\alpha}C^{\beta})$
—	(924)	—	(1)	—	—	—	—	AmIII′ (coil, turns)
943	(945)	4	(5)	—	—	—	—	$\nu(CC^{\alpha})$, AmIII′ (helix)
—	(986)	—	(4)	—	—	—	—	AmIII′ (strand)
1003	(1003)	8	(8)	1003	(1003)	3	(3)	Phe (*F12*)
1031	(1031)	2	(2)	—	—	—	—	Phe (*F18a*)
1054	(1054)	1	(2)	—	—	—	—	sc
1081	(1081)	2	(0.5)	1071	(1071)	1	(1)	ν(CC, CN); Phe
1100	(1100)	2	(0.5)	—	—	—	—	ν(CC, CN)
1127	(1127)	2	(0.5)	—	—	—	—	ν(CC, CN)
1157	(1157)	2	(0.3)	—	—	—	—	$\delta(CH_3)$
—	—	—	—	1178	(1176)	2	(4)	δ(CH rock), Phe
1208	(1208)	2	(2)	1210	(1208)	3	(5)	Phe (*F7a*)
1241	—	3	—	—	—	—	—	AmIII (strand)
1250	(1250)	4	(1)	1261	(1261)	4	(1)	AmIII (strand, coil)
1279	(1279)	4	(2)	1293	—	4	—	AmIII (helix)
1308	(1308)	6	(3)	—	—	—	—	$\delta(CH_2)$, AmIII (helix)
1322	(1322)	7	(3)	—	—	—	—	$\delta(CH_2)$, AmIII (helix)
1342	(1342)	6	(4)	—	—	—	—	sc, $\delta(CH_2)$
—	—	—	—	1393	—	4	—	2 × AmV
1407	(1407)	4	(3)	—	—	—	—	$\nu(COO^-)$
—	(1427)	—	(1)	—	—	—	—	AmII′ (helix)
1451	(1451)	9	(10)	—	—	—	—	$\delta(CH_2)$
—	—	—	—	1457	(1460)	8	(18)	ImideII/II′
—	(1473)	—	(2)	—	(1472)	—	(5)	AmII′
—	—	—	—	1561	(1553)	7	(5)	AmII, $\nu(COO^-)$
1605	(1605)	3	(2)	1604	(1604)	10	(10)	Phe (*F8a*)
—	(1645)	—	(1)	1643	(1635)	6	(8)	AmI′ (helix)
—	(1654)	—	(7)	—	—	—	—	AmI/I′ (helix, coil)
1658	—	10	—	—	—	—	—	AmI (coil, strand)
—	(1674)	—	(1)	1674	(1674)	7	(4)	AmI (strand)

[a] Raman and ultraviolet-resonance Raman (UVRR) data are from spectra of Figs. 2 and 4, respectively, and additional data not shown. Relative intensities are based on an arbitrary 0 to 10 scale, with 10 assigned to the strongest band in the spectrum of the H_2O solution. All data for D_2O solutions are given in parentheses.

[b] Standard three-letter abbreviations are used for amino acids. Detailed vibrational assignments, where known, are indicated as bond stretching (ν) or group deformation (δ) vibrations, or as amide (Am) modes diagnostic of the indicated secondary structure. Italics indicate symbols used for vibrational modes of the phenyl ring of Phe. Further details are given elsewhere (Miura and Thomas, Jr., 1995; Tuma and Thomas, Jr., 2001).

exchange-protected in the native structure. This is consistent with exchange characteristics of the Raman amide bands and with the crystal structure of HUBst, which shows that alanines are located predominantly in regions of α-helical secondary structure.

Raman markers of arginine

Four of the five arginines of HUBst (Arg 53, Arg 55, Arg 58, Arg 61) are located in the DNA-binding domain. A fifth arginine (Arg 37) is located in helix 2 (Fig. 1). To identify Raman markers of these side-chains and signatures of their guanidinium exchanges ($N^{\varepsilon}H \rightarrow N^{\varepsilon}D$, $N^{\eta}H \rightarrow N^{\varepsilon}D$), we examined Raman spectra of L-arginine and poly-L-arginine (PLA) in H_2O and D_2O solutions. The spectrum of L-arginine in H_2O exhibits a pair of arginyl markers at 1054 and 1086 cm^{-1} (Fig. 3, top panel). In PLA these occur at 1072 and 1091 cm^{-1}, respectively (Fig. 3, bottom panel). The bands may be assigned primarily to coupled C-C and C-N skeletal stretching vibrations of the arginyl side-chain, although the effect of peptide bond formation indicates modest coupling with the peptide group in PLA and/or with amino and carboxyl groups in L-arginine. Nevertheless, significant involvement of the guanidinium group is indicated

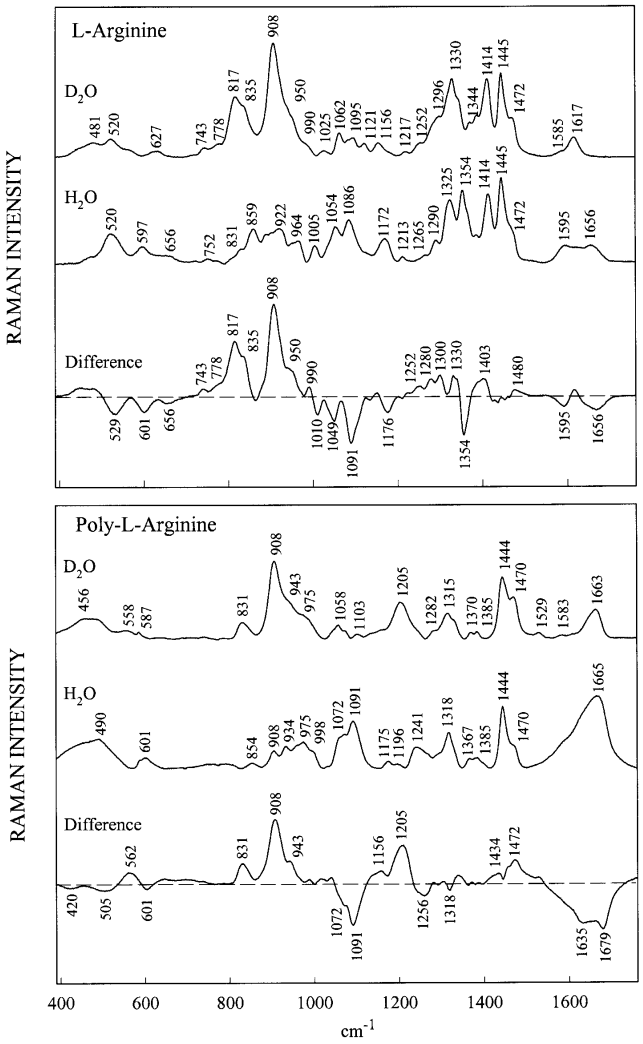

Figure 3. Raman spectra (600 to 1800 cm^{-1}, 532-nm excitation) of solutions of L-arginine (*top*) and poly-L-arginine (*bottom*) at 47 mg/mL. Each panel compares spectra of H_2O (*middle* trace) and D_2O solutions (*top* trace) and the corresponding difference spectrum (*bottom* trace = *top* trace – *middle* trace). Data were normalized to the intensity of the methylene deformation band at 1445 cm^{-1}, which is independent of deuteration (Overman and Thomas, Jr., 1998). Other conditions are as given in the Figure 2 legend.

by the fact that the arginyl markers suffer large intensity changes in D_2O solutions of L-arginine and PLA. The deuterated analogs both exhibit an intense band at 907 ± 1 cm^{-1} and weaker satellites of higher and lower wavenumber values. In the case of PLA, the trio of deuterated arginyl markers (831/907/943 cm^{-1}) is clearly evident in the difference spectrum of the lower panel of Figure 4. Because the 907 cm^{-1} Raman marker is identical in L-arginine and PLA, the band is unlikely to involve significant coupling with the peptide group and may be regarded as diagnostic of the $C^{\beta}H_2$–$C^{\gamma}H_2$–$C^{\delta}H_2$–$N^{\varepsilon}D$–$C^{\zeta}(N^{\eta}D_2)_2$ moiety.

The Raman spectrum of HUBst reveals a deuteration-sensitive band at 1082 cm^{-1} (Fig. 2), which is at the center of gravity of the expected arginyl markers. The band center and deuteration behavior both support assignment to the five arginines per subunit. The apparent coalescence of the expected PLA doublet (1072/1091 cm^{-1}) into a single band in HUBst (1082 cm^{-1}) indicates sensitivity to the side-chain orientations and local environments. Although guanidinium group deuterations in native HUBst are expected to shift the 1082 cm^{-1} band to 907 cm^{-1}, with the attendant appearance in Figure 2D of a difference peak at 907 cm^{-1}, no peak is detected. This can be attributed to cancellation of the expected positive difference intensity by the negative difference intensity accompanying deuteration of the natively exchanged alanines, as discussed in the last paragraph of the preceding section.

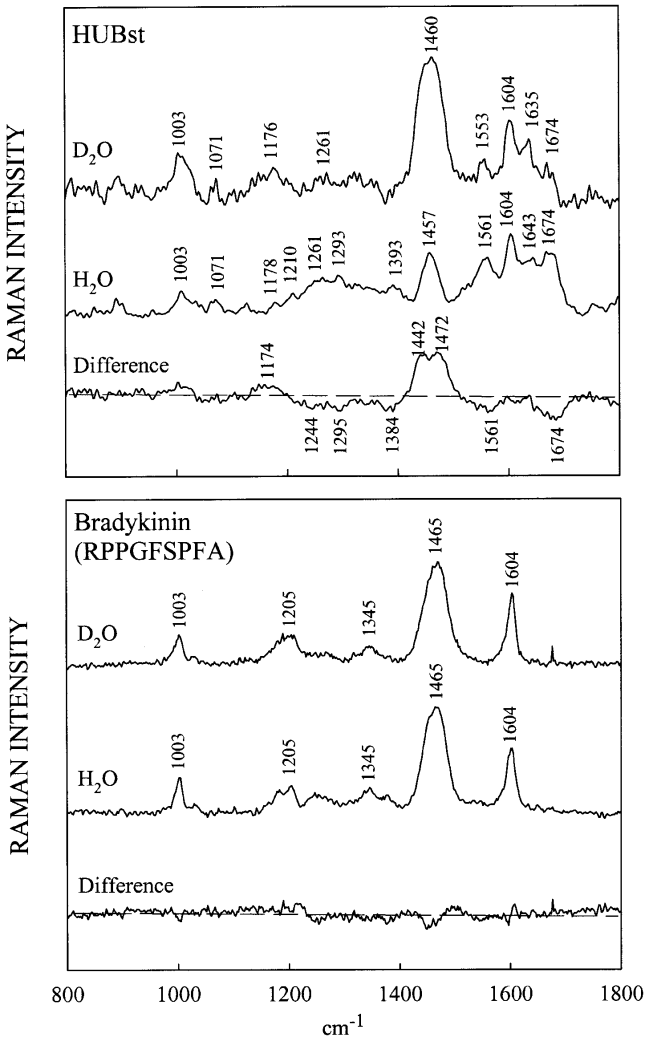

Figure 4. UVRR spectra (800 to 1800 cm^{-1}, 229-nm excitation) of solutions of HUBst (*top*) and bradykinin (*bottom*) at ~2 mg/mL. Each panel compares spectra of H_2O (*middle* trace) and D_2O solutions (*top* trace) and their corresponding difference spectrum (*bottom* trace = *top* trace–*middle* trace). Other conditions are as given in the Figure 2 legend.

Raman markers of other HUBst side-chains

In addition to alanine and arginine, the four phenylalanines per subunit are prolific contributors to the Raman spectra of HUBst (Table 1). The only other amino acid type for which a specific spectral contribution can be proposed is methionine. Thus, the weak band at 701 cm^{-1} and the medium intensity band at 743 cm^{-1} are likely to involve C^{γ}-S stretching vibrations of the Met 1 and Met 69 side-chains. Previously proposed correlations (Nogami et al. 1975a,b) indicate that the torsion χ^3 (C^{β}–C^{γ}–S–C^{ε}) of each Met side-chain is in the *trans* range. The 701-cm^{-1} marker is well isolated from other bands and might provide a useful probe of changes in methionine local environment with DNA binding. Met 69 has been proposed as a DNA recognition element, possibly intercalating into the minor groove of bound DNA (White et al. 1999).

Although aliphatic side-chains make many additional contributions to the HUBst Raman spectra of Figure 2, their bands overlap one another extensively, and detailed amino acid assignments are not feasible. Several such bands and their group vibrational characteristics are listed in Table 1.

UVRR markers of HUBst secondary structure and side-chains

The 229-nm excited UVRR spectra of HUBst in H_2O and D_2O solutions are compared in the top panel of Figure 4. The dominant effect of native-state deuteration, as reflected in the UVRR spectrum, is enhancement of the amide II′ intensity. This is represented by the twin difference peaks at 1442 and 1472 cm^{-1}, which result from exchange of irregular and β-strand conformations, respectively. In accord with previous studies of model compounds (Austin et al. 1993; Chi et al. 1998), the diminished amide I intensity at 1674 cm^{-1} and diminished amide II intensity at 1561 cm^{-1} are also attributable to native exchange of the non–α-helical peptide sites. Exchange-protected α-helical sites are identified by the UVRR amide II α-helix marker that persists at 1553 cm^{-1} in the D_2O solution spectrum of Figure 4. Other peaks and troughs in the Figure 4 difference spectrum are of marginal amplitudes and may reflect experimental error or slightly different UVRR cross sections for side-chain markers in the nondeuterated and deuterated forms of HUBst.

Intensities of the UVRR amide II bands in native and natively exchanged HUBst (Fig. 4, top panel) allow a semiquantitative estimate of the extent of peptide NH → ND exchange. Thus, the amide II marker (1561 cm^{-1}) of HUBst in H_2O solution, which comprises contributions from all types of secondary structure, is replaced in the natively exchanged protein by an intense amide II′ doublet (difference peaks at 1442 and 1472 cm^{-1}; Austin et al. 1993). Peptide sites that remain protected from native exchange account for the residual amide II intensity at 1553 cm^{-1} (Chi et al. 1998). These results indicate that ~80% of the peptide sites undergo NH → ND exchange, in agreement with the off-resonance Raman data of Figure 2. As noted in the next section, the prominent UVRR band observed at 1457 cm^{-1} for HUBst in H_2O solution (Fig. 4, top panel, middle trace) is owing to proline residues.

UVRR marker of proline

The UVRR spectrum of HUBst in H_2O reveals an intense and broad band near 1457 cm^{-1} (Fig. 4, top panel, middle trace). On the basis of 240-nm UVRR studies of prolyl-containing peptides, Takeuchi and Harada (1990) assigned such a band to the imide II mode of the X-Pro peptide linkage. To confirm this assignment for 229-nm UVRR excitation, we obtained spectra of the prolyl-rich peptide bradykinin (Fig. 4, lower panel). The data of Figure 4 indicate that the 1457-cm^{-1} band of HUBst is the counterpart of the imide II mode of bradykinin (1465 cm^{-1}). The lower wavenumber of the imide II marker in HUBst can be attributed to weaker hydrogen bonding of prolyl C=O sites in HUBst vis-à-vis bradykinin. (Limits observed for the imide II mode are ~1445 cm^{-1} for a non–hydrogen-bonded C=O group and 1485 cm^{-1} for a very strongly hydrogen-bonded C=O acceptor; Takeuchi and Harada 1990). Accordingly, the imide II marker of HUBst at 1457 cm^{-1} is diagnostic of relatively weak prolyl C=O interactions in the native protein.

The bradykinin UVRR data of Figure 4 show that with 229-nm excitation, the prolyl imide II marker is intrinsically more intense than phenylalanyl markers near 1604 and 1003 cm^{-1}. The absence of any deuteration shift indicates further that the marker represents a highly localized vibration of the proline moiety. We note that the UVRR band intensity ratios for Pro and Phe markers in the H_2O solution spectrum of HUBst are as expected for the Pro:Phe residue distribution (1:1) in the protein. In addition, all of the UVRR intensity increase observed in the 1440- to 1480-cm^{-1} interval accompanying HUBst deuteration can be attributed with confidence to nonprolyl peptide exchange (i.e., amide II′).

Discussion

Solution conformation of HUBst

The NMR solution structure of dimeric HUBst reveals a DNA-binding motif consisting of two extended but flexible arms (residues 55–74) anchored to a hydrophobic α-helical core (Fig. 1; Boelens et al. 1996). The NMR structural model contains 37% α-helix and ~16% β-strand. The remaining 47% of the NMR structure is presumed to consist of nonrepetitive or irregular conformations. The α-helix content in the X-ray crystal structure is in agreement with the NMR solution structure (White et al. 1999), although the

X-ray structure is not of sufficient resolution to resolve details of β-strand or other conformations in the C-terminal arms. Quantitative analyses of the Raman amide I (Berjot et al. 1987) and amide III′ (Tuma and Thomas, Jr., 1997) data of Figures 2 and 3 confirm the high α-helix content of the solution structure and indicate considerably more β-strand than inferred by NMR (26% versus 16%). The difference between the NMR- and Raman-based models represents eight (± two) additional residues per subunit in regions of β-strand at the expense of irregular conformations. Because the nonhelical residues are located principally in the C-terminal arms of the subunit, we propose that these arms are more highly β-stranded than inferred initially by NMR. A recent refinement of both the NMR (Boelens et al. 1996) and X-ray (White et al. 1999) models supports this hypothesis and attributes the initial under-assessment of β-strand content to the overall mobility of the C-terminal arms (Raves et al. 2001).

Dynamics and interactions of the HUBst dimer

Measurements of peptide H/D exchange provide a window into protein intramolecular dynamics and the surface area impacted by quaternary interactions (Englander et al. 1996; Englander 2000). We have found that ~80% of the peptide sites of the HUBst dimer undergo NH → ND exchange. This is surprising when compared with the percentage (17%) of dimer surface area that is expected to be exposed to solvent. The ratio of exposed to total subunit area is estimated as 0.167, using the relation of Miller et al. (1987), that is, $4.5 \cdot M^{0.76}/1.48 \cdot M = 4840$ Å^2/28,860 Å^2, where M is the subunit molecular weight of 9.75 kD (Wilson et al. 1990). The much greater than expected exchange limit of the HUBst dimer, which reflects substantial exchange of α-helical regions as well as complete exchange of nonhelical regions, implies that peptide exchange dynamics extend to α-helices at the subunit interface (Englander et al. 1996; Englander 2000). Exchange at the interface presumably reflects pleomorphism in the native dimer that may be required for efficient non-specific binding to DNA. Similar NH → ND exchange characteristics have been observed for other protein quaternary assemblies (Tuma et al. 1996, 1998, 1999).

Raman markers of residues conserved among HU proteins

The Raman signature of HUBst exhibits identifiable spectral markers (Table 1) of residues that are conserved among many bacterial histone-like proteins, including arginines (Arg 53, Arg 55, Arg 58, Arg 61) that line the DNA interface and prolines (Pro 63, Pro 72) and methionine (Met 69) that are at or near the distal loops of the DNA-binding arms (Williams and Maher III 2000). These residues are critical to HU function (Saitoh et al. 1999), and their Raman markers provide a convenient basis for probing HU/DNA recognition in nucleoprotein complexes. In addition, the deficiency of aromatic side-chains in HUBst, specifically the absence of both Trp and Tyr residues, facilitates the identification of Raman markers of key aliphatic side-chains. The abundant and largely conserved Ala residues of HUBst (Fig. 1), which function in α-helix packing, also exhibit an identifiable Raman signature and a diagnostic pattern of alanyl peptide exchange. Because alanines of HU proteins have been correlated with protein thermostability (Wilson et al. 1990), the Raman procedures developed here are expected to be useful in assessing the roles of local alanyl environments in subunit stability and assembly. The present study reveals that eight alanyl sites in α-helices 1 and 2 of the HUBst dimer are exchange protected in the native subunit fold, consistent with strong N-H…O hydrogen bonding of the peptides. It will be of interest to probe the dynamics and interactions of these Ala sites in the HUBst:DNA complex, as well as in other protein/DNA complexes.

Structural studies of several families of DNA-binding architectural factors, including the histone-like proteins HU and IHF, as well as HMG-box and winged-helix proteins, illustrate how modest differences among members of the same family determine specificity in the mechanism of DNA recognition (Gajiwala and Burley 2000; Travers 2000). Although HU and IHF have high sequence and structure homology, HU is distinguished from IHF by its ability to induce superhelical stress in covalently closed DNA duplexes (Ogata et al. 1997). The different outcomes of HU/DNA and IHF/DNA recognition may be distinguishable by sensitive Raman difference methods, which have the capacity to differentiate even modestly supercoiled DNA from relaxed DNA (Serban et al. 2002). The present findings represent a starting point for subsequent Raman and UVRR investigation of HU:DNA and IHF:DNA complexes and comparative analysis of their respective molecular mechanisms of interaction with topological variants of high-molecular-weight DNA. These studies also provide a basis for future application of Raman methods to other proteins containing alanyl and prolyl residues at inter-subunit and subunit/DNA interfaces.

Materials and methods

Sample preparation and purification

Biochemicals and reagents were obtained from Sigma and Cambridge Isotope Laboratories. HUBst protein was isolated and purified from transformed *Escherichia coli* BL21(DE3)pLysS cells using standard procedures (Padas et al. 1992). Briefly, the cells were grown at 37°C in LB medium containing ampicillin and chloramphenicol (50 μg/mL) to mid-log phase (0.5 O.D.$_{600}$). Full induction was achieved by addition of IPTG at 1 mM final concentration. Cells were grown for 7 h at 37°C after induction and

harvested by centrifugation for 10 min at 6,000 rpm (Beckman Avanti J-20 centrifuge, JLA-8.1 rotor). The harvested cells (~12 g/L culture medium) were washed with 20 mM Tris, 100 mM NaCl, and 0.1 mM PMSF (pH 7.5) and lysed by sonication (Branson Sonifier 450). Subsequent procedures were carried out at 4 °C. The sonicate was centrifuged for 1 h at 45,000 rpm (Beckman L70 ultracentrifuge, Ti50.2 rotor), and proteins in the supernatant were fractionated by precipitation in saturated $(NH_4)_2SO_4$ and centrifuged for 20 min at 45,000 rpm. The resulting supernatant was dialyzed against 8 L of 10 mM sodium phosphate, 0.1 mM PMSF, 0.1 mM EDTA (pH 7.5; buffer A) and applied to a CM-Sepharose column (1.5 × 20cm, Amersham Pharmacia Biotech). HUBst was eluted with a linear gradient of 0 to 500 mM NaCl in buffer A, and the pooled fractions containing HUBst (ε_{230} = 2.3 mL/mg/cm and ε_{280} = 0.56 mL/mg/cm) were dialyzed against 100 mM Na phosphate, 100 mM NaCl, 0.1 mM PMSF, 0.1 mM EDTA (pH 7.5; buffer B). The protein was subsequently applied to a Bio-Scale S5 column (BioRad) and eluted with a linear gradient of 0.1 to 1.0 M Na phosphate in buffer B. The purified HUBst fractions were analyzed by SDS-PAGE and dialyzed against 20 mM Tris and 50 mM NaCl (pH 7.5). Finally, the protein was either concentrated in this buffer for use in unfolding/refolding experiments or exchanged with 100 mM NaCl solution and then concentrated using a Centricon-3 ultrafiltrator of 3,000-Da cutoff (Amicon, Inc.) for use in Raman analyses. The concentration of purified HUBst was determined by UV absorbance using a molar extinction coefficient at 258 nm of ε_{258} = 0.076 mL/mg/cm (1482 $M^{-1} \cdot cm^{-1}$; Welfle et al. 1992).

Deuterium exchange

Deuterium exchange of native HUBst was carried out by incubation in either 100 mM NaCl/D_2O (at pD 7.9) or 10 mM Tris, 50 mM NaCl/D_2O (pD 7.9) for 4 h at 20 °C. This procedure accomplishes H/D exchange of labile main-chain (peptide NH → ND) and side-chain sites (e.g., Lys and Arg) not protected by the native fold. Complete H/D exchange of all labile sites was accomplished by incubating the unfolded protein for 1 h in 6 M guanidinium deuteriochloride (GuDCl). The fully exchanged protein was subsequently refolded by extensive dialysis against 10 mM Tris, 50 mM NaCl/D_2O (pD 7.9) and concentrated on a Centricon-3 ultrafiltrator as required for Raman spectroscopy. Completion of H/D exchange was assessed by elimination of Raman intensity owing to NH and OH group hydrogenic stretching modes (3200 to 3400 cm^{-1}). The integrity of the refolded protein was assessed by restoration of the CD profile associated with the native structure. The unfolding/refolding cycle using nondeuterated reagents was also shown to restore the Raman signature of the native structure. H/D exchanges of model proteins (bradykinin, PLA, and related amino acids) were carried out similarly.

Raman spectroscopy

Raman spectra of HUBst were obtained from H_2O (D_2O) solutions prepared at 20 μg/μL in either 0.1 M NaCl (pH 7.5, pD 7.9) or 10 mM Tris, 50 mM NaCl (pH 7.5, pD 7.9). Solutions of L-arginine and PLA were prepared at 5 mM and adjusted to pH 7.5 (pD 7.9) with HCl (DCl) or NaOH (NaOD). Aliquots of ~5 μL were sealed in glass capillaries (KIMAX No. 34507) and thermostated at 20 °C (Thomas, Jr., and Barylski 1970) for data collections. Spectra were excited at 532 nm by using a solid-state Nd:YVO_4 laser (Verdi, Coherent, Inc.) and collected on a Spex 500 M single spectrograph (Instruments S.A.) equipped with a holographic notch filter and liquid nitrogen–cooled, back-thinned, charge-coupled-device (CCD) detector of 2000 × 800 pixels (Spectrum One, Instruments S.A.). The radiant power at the sample was ~30 mW. The effective spectral resolution was 3 cm^{-1}. Raman frequencies are accurate to ±0.5 cm^{-1}, as judged by calibration of the spectrophotometer using the 459.5 cm^{-1} band of CCl_4. Spectra shown below are the accumulated averages of 10 to 30 exposures of 40 s each. Further details of the instrumentation and data collection protocols are given elsewhere (Movileanu et al. 1999).

UVRR spectroscopy

UVRR spectra were excited with ≤1 mW of 229-nm radiation from an Innova 300 FreD argon laser (Coherent, Inc.) and were collected on a Spex model 750M single-grating (2400 g/mm) spectrograph equipped with a Spex model Spectrum-1 liquid nitrogen–cooled CCD detector (ISA). Spectrometer resolution (8 cm^{-1}), wavenumber calibration (versus CCl_3CN), and performance characteristics have been described (Russell et al. 1995). UVRR spectra were collected from H_2O (D_2O) solutions of HUBst prepared at 2 μg/μL in 10 mM Tris (pH 7.5, pD 7.9). Samples were maintained at room temperature (20 °C) in a rotating quartz cell (300 rpm).

The prominent UVRR band from phenylalanines of HUBst (1003 cm^{-1}) also serves as an internal frequency and intensity standard. The reported spectral data represent averages obtained from five independent experiments, which exhibited band intensity deviations generally not exceeding ±5% and wavenumber deviations not exceeding ±1 cm^{-1} for sharp bands or ±4 cm^{-1} for broad or very weak bands. As in previous work (Russell et al. 1995; Wen et al. 1997), no photochemical damage was observed for any sample as judged by the absence of transient or irreversible changes in the UVRR spectra within the time of data collection (<10 min). Exposure thresholds for photochemical decomposition (>12 min) were established for each sample at the laser power used and were never exceeded. Other potential sources of error, such as polarization artifacts and sample self-absorption effects, are minimized by the experimental design and collection protocols, as detailed elsewhere (Russell et al. 1995; Wen et al. 1997; Wen and Thomas, Jr., 1998).

CD spectroscopy

CD spectra were recorded from HUBst solutions (~0.3 mg/mL in 1 mM sodium cacodylate buffer at pH 7.0, 20°C) using a Jasco J-720 spectropolarimeter (Japan Spectroscopic, Co.) and an optical path of 0.1 cm. The spectropolarimeter was calibrated using ammonium *d*-camphor-10-sulfonate. CD data referenced below represent the accumulated averages of five scans, each obtained at a scan rate of 0.5 nm/sec.

Acknowledgments

Support of this research by grant GM54378 (to G.J.T.) from the National Institutes of Health is gratefully acknowledged. D.S. also thanks Dr. James M. Benevides for helpful discussions and assistance throughout this project.

The publication costs of this article were defrayed in part by payment of page charges. This article must therefore be hereby marked "advertisement" in accordance with 18 USC section 1734 solely to indicate this fact.

References

Austin, J.C., Jordan, T., and Spiro, T.G. 1993. Ultraviolet resonance Raman studies of proteins and related compounds. In *Biomolecular spectroscopy, Part A*. (eds. R.J.H. Clark and R.E. Hester), pp. 55–127. John Wiley and Sons, New York.

Bandekar, J. 1992. Amide modes and protein conformation. *Biochim. Biophys. Acta* **1120:** 123–143.

Benevides, J.M., Chan, G., Lu, X.J., Olson, W.K., Weiss, M.A., and Thomas, Jr., G.J. 2000a. Protein-directed DNA structure, I: Raman spectroscopy of a high-mobility-group box with application to human sex reversal. *Biochemistry* **39:** 537–547.

Benevides, J.M., Li, T., Lu, X.J., Srinivasan, A.R., Olson, W.K., Weiss, M.A., and Thomas, Jr., G.J. 2000b. Protein-directed DNA structure, II: Raman spectroscopy of a leucine zipper bZIP complex. *Biochemistry* **39:** 548–556.

Berjot, M., Marx, J., and Alix, A.J.P. 1987. Determination of the secondary structure of proteins from the Raman amide I band: The reference intensity profiles method. *J. Raman Spectrosc.* **18:** 289–300.

Bewley, C.A., Gronenborn, A.M., and Clore, G.M. 1998. Minor groove-binding architectural proteins: Structure, function, and DNA recognition. *Annu. Rev. Biophys. Biomol. Struct.* **27:** 105–131.

Boelens, R., Vis, H., Vorgias, C.E., Wilson, K.S., and Kaptein, R. 1996. Structure and dynamics of the DNA binding protein HU from *Bacillus stearothermophilus* by NMR spectroscopy. *Biopolymers* **40:** 553–559.

Chi, Z., Chen, X.G., Holtz, J.S., and Asher, S.A. 1998. UV resonance Raman-selective amide vibrational enhancement: Quantitative methodology for determining protein secondary structure. *Biochemistry* **37:** 2854–2864.

Drlica, K. and Rouviere-Yaniv, J. 1987. Histonelike proteins of bacteria. *Microbiol. Rev.* **51:** 301–319.

Englander, S.W. 2000. Protein folding intermediates and pathways studied by hydrogen exchange. *Annu. Rev. Biophys. Biomol. Struct.* **29:** 213–238.

Englander, S.W., Sosnick, T.R., Englander, J.J., and Mayne, L. 1996. Mechanisms and uses of hydrogen exchange. *Curr. Opin. Struct. Biol.* **6:** 18–23.

Esser, D., Rudolph, R., Jaenicke, R., and Bohm, G. 1999. The HU protein from *Thermotoga maritima*: Recombinant expression, purification and physicochemical characterization of an extremely hyperthermophilic DNA-binding protein. *J. Mol. Biol.* **291:** 1135–1146.

Gajiwala, K.S. and Burley, S.K. 2000. Winged helix proteins. *Curr. Opin. Struct. Biol.* **10:** 110–116.

Holbrook, J.A., Tsodikov, O.V., Saecker, R.M., and Record, Jr., M.T. 2001. Specific and non-specific interactions of integration host factor with DNA: Thermodynamic evidence for disruption of multiple IHF surface salt-bridges coupled to DNA binding. *J. Mol. Biol.* **310:** 379–401.

Lee, S.-H. and Krimm, S. 1998. Ab initio–based vibrational analysis of α-poly(L-alanine). *Biopolymers* **46:** 283–317.

Luisi, B. 1995. DNA-protein interaction at high resolution. In *DNA-protein: Structural interactions*. (ed. D.M.J. Lilley), pp. 1–48. IRL Press at Oxford University Press, Oxford, U.K.

Miller, S., Lesk, A.M., Janin, J., and Chothia, C. 1987. The accessible surface area and stability of oligomeric proteins. *Nature* **328:** 834–835.

Miura, T. and Thomas, Jr., G.J. 1995. Raman spectroscopy of proteins and their assemblies. In *Subcellular biochemistry. Proteins: Structure, function and engineering*, Vol. 24. (eds. B. B. Biswas and S. Roy), pp. 55–99. Plenum, New York.

Movileanu, L., Benevides, J.M., and Thomas, Jr., G.J. 1999. Temperature dependence of the Raman spectrum of DNA, I: Raman signatures of premelting and melting transitions of poly(dA-dT) · poly(dA-dT). *J. Raman Spectrosc.* **30:** 637–649.

Nogami, N., Sugeta, H., and Miyazawa, T. 1975a. C-S stretching vibrations and molecular conformations of isobutyl methyl sulfide and related alkyl sulfides. *Bull. Chem. Soc. Jpn.* **48:** 2417–2420.

———. 1975b. C-S stretching vibrations and molecular conformations of methyl propyl sulfide and related alkyl sulfides. *Chem. Lett.* **2:** 147–150.

Ogata, Y., Inoue, R., Mizushima, T., Kano, Y., Miki, T., and Sekimizu, K. 1997. Heat shock-induced excessive relaxation of DNA in *Escherichia coli* mutants lacking the histone-like protein HU. *Biochim. Biophys. Acta* **1353:** 298–306.

Overman, S.A. and Thomas, Jr., G.J. 1998. Amide modes of the α-helix: Raman spectroscopy of filamentous virus fd containing peptide ^{13}C and ^{2}H labels in coat protein subunits. *Biochemistry* **37:** 5654–5665.

Padas, P.M., Wilson, K.S., and Vorgias, C.E. 1992. The DNA-binding protein HU from mesophilic and thermophilic bacilli: Gene cloning, overproduction and purification. *Gene* **117:** 39–44.

Raves, M.L., Doreleijer, J.F., Vis, H., Vorgias, C.E., Wilson, K.S., and Kaptein, R. 2001. Joint refinement as a tool for thorough comparison between NMR and X-ray data and structures of HU protein. *J. Biomol. NMR* **21:** 235–248.

Rice, P.A. 1997. Making DNA do a U-turn: IHF and related proteins. *Curr. Opin. Struct. Biol.* **7:** 86–93.

Rice, P.A., Yang, S., Mizuuchi, K., and Nash, H.A. 1996. Crystal structure of an IHF-DNA complex: A protein-induced DNA U-turn. *Cell* **87:** 1295–1306.

Russell, M.P., Vohník, S., and Thomas, Jr., G.J. 1995. Design and performance of an ultraviolet resonance Raman spectrometer for proteins and nucleic acids. *Biophys. J.* **68:** 1607–1612.

Saitoh, F., Kawamura, S., Yamasaki, N., Tanaka, I., and Kimura, M. 1999. Arginine-55 in the β-arm is essential for the activity of DNA-binding protein HU from *Bacillus stearothermophilus*. *Biosci. Biotechnol. Biochem.* **63:** 2232–2235.

Schneider, G.J., Sayre, M.H., and Geiduschek, E.P. 1991. DNA-bending properties of TF1. *J. Mol. Biol.* **221:** 777–794.

Serban, D., Benevides, J.M., and Thomas, Jr., G.J. 2002. DNA secondary structure and Raman markers of supercoiling in *Escherichia coli* plasmid pUC19. *Biochemistry* **41:** 847–853.

Sutton, P. and Koenig, J.L. 1970. Raman spectra of L-alanine oligomers. *Biopolymers* **9:** 615–634.

Takeuchi, H. and Harada, I. 1990. Ultraviolet resonance Raman spectroscopy of X-proline bonds: A new marker band of hydrogen bonding at the imide C=O site. *J. Raman Spectrosc.* **21:** 509–515.

Thomas, Jr., G.J. and Barylski, J. 1970. Thermostating capillary cells for a laser-Raman spectrophotometer. *Appl. Spectrosc.* **24:** 463–464.

Travers, A. 2000. Recognition of distorted DNA structures by HMG domains. *Curr. Opin. Struct. Biol.* **10:** 102–109.

Tuma, R. and Thomas, Jr., G.J. 1997. Mechanisms of virus assembly probed by Raman spectroscopy: The icosahedral bacteriophage P22. *Biophys. Chem.* **68:** 17–31.

———. 2002. Raman spectroscopy of viruses. In: *Handbook of vibrational spectroscopy: Applications of vibrational spectroscopy in biochemistry, biomedicine and pharmaceutical science*, Vol. 5. (eds. J.M. Chalmers and P.R. Griffiths), pp. 3519–3535. John Wiley & Sons, Chichester, UK.

Tuma, R., Bamford, J.K.H., Bamford, D.H., Russell, M.P., and Thomas, Jr., G.J. 1996. Structure, interactions and dynamics of PRD1 virus, I: Coupling of subunit folding and capsid assembly. *J. Mol. Biol.* **257:** 87–101.

Tuma, R., Prevelige, Jr., P.E., and Thomas, Jr., G.J. 1998. Mechanism of capsid maturation in a double-stranded DNA virus. *Proc. Natl. Acad. Sci.* **95:** 9885–9890.

Tuma, R., Bamford, J.K., Bamford, D.H., and Thomas, Jr., G.J. 1999. Assembly dynamics of the nucleocapsid shell subunit (P8) of bacteriophage φ6. *Biochemistry* **38:** 15025–15033.

Tuma, R., Tsuruta, H., Benevides, J.M., Prevelige, Jr., P.E. and Thomas, Jr., G.J. 2001. Characterization of subunit structural changes accompanying assembly of the bacteriophage P22 procapsid. *Biochemistry* **40:** 665–674.

Welfle, H., Misselwitz, R., Welfle, K., Groch, N., and Heinemann, U. 1992. Salt-dependent and protein-concentration-dependent changes in the solution structure of the DNA-binding histone-like protein, HBsu, from *Bacillus subtilis*. *Eur. J. Biochem.* **204:** 1049–1055.

Wen, Z.Q. and Thomas, Jr., G.J. 1998. Ultraviolet resonance Raman spectroscopy of DNA and protein constituents of viruses: Assignments and cross sections for excitations at 257, 244, 238 and 229 nm. *Biopolymers* **45:** 247–256.

Wen, Z.Q., Overman, S.A., and Thomas, Jr., G.J. 1997. Structure and interactions of the single-stranded DNA genome of filamentous virus fd: Investigation by ultraviolet resonance Raman spectroscopy. *Biochemistry* **36:** 7810–7820.

Werner, M.H., Gronenborn, A.M., and Clore, G.M. 1996. Intercalation, DNA kinking, and the control of transcription. *Science* **271:** 778–784.

White, S.W., Appelt, K., Wilson, K.S., and Tanaka, I. 1989. A protein structural motif that bends DNA. *Proteins* **5:** 281–288.

White, S.W., Wilson, K.S., Appelt, K., and Tanaka, I. 1999. The high-resolution structure of DNA-binding protein HU from *Bacillus stearothermophilus*. *Acta Crystallogr. D. Biol. Crystallogr.* **55 (Pt 4):** 801–809.

Williams, L.D. and Maher III, L.J. 2000. Electrostatic mechanisms of DNA deformation. *Annu. Rev. Biophys. Biomol. Struct.* **29:** 497–521.

Wilson, K.S., Vorgias, C.E., Tanaka, I., White, S.W., and Kimura, M. 1990. The thermostability of DNA-binding protein HU from bacilli. *Protein Eng* **4:** 11–22.